Article

Polymer-Based Microring Resonator with the Multimode Interference Coupler Operating at Very-Near-Infrared Wavelengths

Huanlin Lv [1,2], **Yuxin Liang** [1] , **Zhenlin Wu** [1], **Xiuyou Han** [1], **Geert Morthier** [3] **and Mingshan Zhao** [2,*]

[1] School of Optoelectronic Engineering and Instrumentation Science, Dalian University of Technology, Dalian 116023, China
[2] School of information Science and Engineering, Dalian Polytechnic University, Dalian 116034, China
[3] Photonics Research Group, Department of Information and Technology, Ghent University, 9000 Ghent, Belgium
* Correspondence: mszhao@dlut.edu.cn; Tel.: +86-0411-8470-6491

check for updates

Abstract: A microring resonator with the multimode interference coupler is fabricated on the polymer platform by using UV-based soft nanoimprint technique. A unique class of fluorinated polymer, perfluoropolyether (PFPE), is employed for the fabrication of the flexible soft mold. By optimizing the proportion between Ormocore and the thinner maT, the microring resonator is fabricated almost without residual layer. The fabricated device with a Q-factor up to 2.3×10^4 is demonstrated for very-near-infrared wavelengths, which shows high potential for sensing applications.

Keywords: microring resonator; polymer waveguide; multimode interference coupler (MMI); UV-based soft nanoimprint

1. Introduction

Integrated optics has been playing important roles in the optics communication and sensing areas in recent years. Among different structures, microring resonators are the key and fundamental components as they can provide resonances with high Q factor and extinction ratio (ER). A variety of integrated optical devices have been reported based on microring resonators, such as filters [1,2], modulators [3,4], and lasers [5,6]. Except for the applications in optical communication, microring resonators have also been applied in the sensing area [7,8]. Because of the resonance effect, the sensitivity can be much improved. A microring resonator is normally composed of a microring and one or two straight waveguides which are used as input and output ports. Two kinds of couplers are used to couple the light between the straight waveguides and microring: directional coupler [9] and MMI (multimode interference) coupler [10]. The directional coupler is composed of two parallel waveguides, and the coupling efficiency can be adjusted continuously by changing the coupling length. However, since the coupling gap is very small, the fabrication is difficult. The MMI coupler is based on the self-imaging effect. It has advantages such as high fabrication tolerance and insensitivity to the wavelength and the polarization. However, it can just reach several fixed coupling ratios by adjusting the structure of the multimode waveguide.

Microring resonators have been demonstrated on different optical materials such as silicon-on-insulator (SOI) [11], Si_xN_y [12,13], and polymers [14–16]. Compared with conventional inorganic materials, polymers as organic materials have advantages such as low cost, high optical transmittance, and simple fabrication processes [17,18]. Moreover, different unique properties such as low loss and high electro-optic coefficient can be achieved by operating on molecular scale during

chemical synthesis [19,20]. As for the fabrication, several simple and productive processes have been proposed, such as UV lithography [21], direct laser writing [22], and nanoimprint lithography (NIL) [23]. Among them, NIL has drawn much attention as it can achieve high resolution and high yield at the same time with simple processes. By using a mechanical imprinting process, one can avoid the diffraction limit which is inevitable in the UV lithography and reach a high resolution. Since it is based on the replication technology, the quality of the master mold is very important. The traditional NIL utilizes a hard mold which is fabricated on the silicon or metal platform. However, after several imprints, the hard mold usually gets damaged and contaminated, which influences its reutilization. In order to solve this problem, UV-based soft nanoimprint lithography (UV Soft NIL) is proposed [24]. The soft mold which is replicated from the hard mold is introduced to do the imprinting. As the soft mold normally has low surface energy, the replication process will not bring damage to the hard mold and the demolding process can also be much easier. On the other hand, as UV curing is chosen, high pressure and temperature are no longer needed. Polydimethylsiloxane (PDMS) has demonstrated its advantages as soft mold in the UV Soft NIL due to its advantages such as flexible backbone structure, high degree of toughness, and large elongation. However, in recent years, a new material, Polyterafluoroethylene (PFPE) is proposed as soft mold [25]. It has lower surface energy and ideal elastic modulus which makes it a better option for the soft mold. The resolution of the UV Soft NIL can reach 20 nm, and it also can achieve a high yield by using the roll-to-roll process [26,27].

In this work, a microring resonator with MMI coupler was demonstrated on the low-cost polymer platform. OrmoCore (Microresist Technology), which has a low loss at short wavelengths was utilized. The very-near-infrared region (around 890 nm) was chosen as the working wavelengths, since the absorption loss of water in this wavelength region is much lower than at the optical fiber communication wavelengths. In addition, the light sources and detectors are also cheaper. The microring resonator was fabricated by Soft UV NIL which is a cost-effective and high-throughput technique. PFPE with very low surface energy was used to fabricate the soft mold. A 3 dB MMI coupler was designed to couple the light between the straight waveguide and the microring. In order to reduce the thickness of the residual layer to a desired level, the volume ratio of OrmoCore and the thinner maT was optimized. The fabricated device with a Q-factor up to 2.3×10^4 showed high potential for sensing applications.

2. Structure and Design

The microring resonator with MMI coupler is illustrated in the Figure 1a. The light is launched in through the input waveguide and then coupled into the microring by the MMI coupler. The resonance will take place at the periodic and specific wavelengths, which are named resonance wavelengths. The cross-section of the polymer-based ridge waveguide is shown in Figure 1b. The polymer, OrmoCore, was utilized as it has a low absorption loss at short wavelengths [28]. The refractive index (RI) is 1.543 at the wavelength of 890 nm. The under cladding is SiO_2 with the RI of 1.453. The upper cladding is assumed as water solution with the RI of 1.33 for biochemical sensing applications. In the imprinting process, the core layer cannot be completely squeezed out and is finally left as the residual layer. It will increase the bend loss of the microring and further decrease the Q factor and ER. The width and height of the waveguide were designed with the same value 1 μm in order to support the single-mode condition.
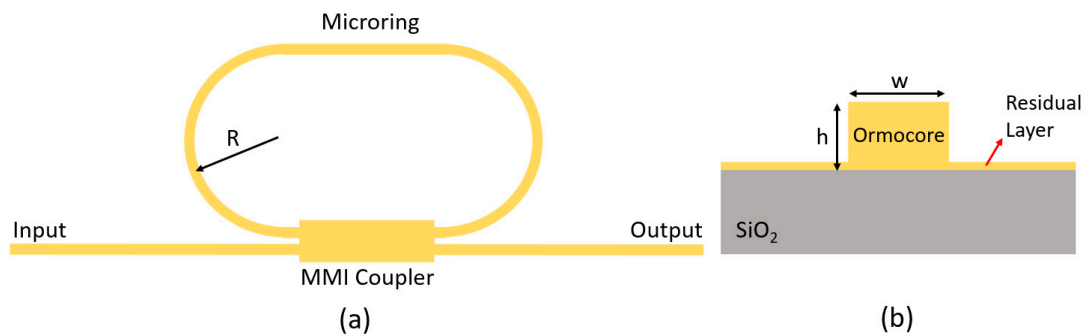
Figure 1. (**a**) The schematic configuration of microring resonator with multimode interference (MMI) coupler; (**b**) The cross-section of the polymer-based ridge waveguide.

The Q factor is a key parameter for the microring resonators and low loss will lead to a high Q factor. Therefore, the bend loss of the microring needs to be optimized. The relationship between bend loss and the microring radius, R, was simulated with Rsoft, and the result is shown in Figure 2. It can be seen that the bend loss will decrease sharply and then tend to be 0 gradually with increasing radius. Figure 2 also shows that there is almost no extra bend loss when R = 220 μm, which was chosen as the radius of the microring resonator.
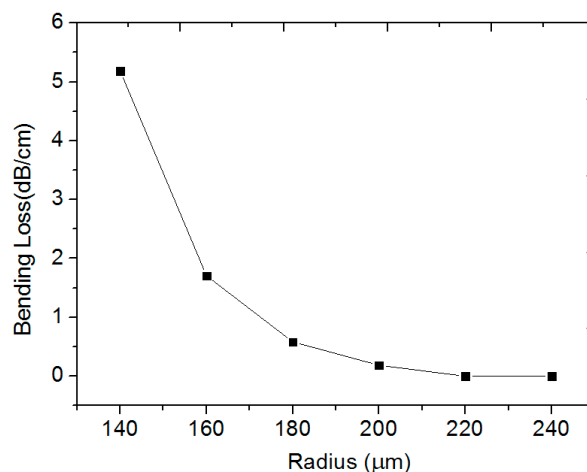

Figure 2. The relationship between bend loss and the radius of the microring.

The MMI coupler is based on the self-imaging effect and its operation principle can be described as below. The input optical field excites the modes in the multimode waveguide at the junction between input waveguide and multimode waveguide. At periodic intervals along the propagation direction, the modes will overlay with each other and finally form single or multiple images of the input optical field [29]. By placing output waveguides at the positions of the images, couplers with different coupling efficiencies can be obtained. The structure of the MMI coupler is shown in Figure 3. L and W are the length and width of the multimode waveguide. D is the separation distance between the output ports.
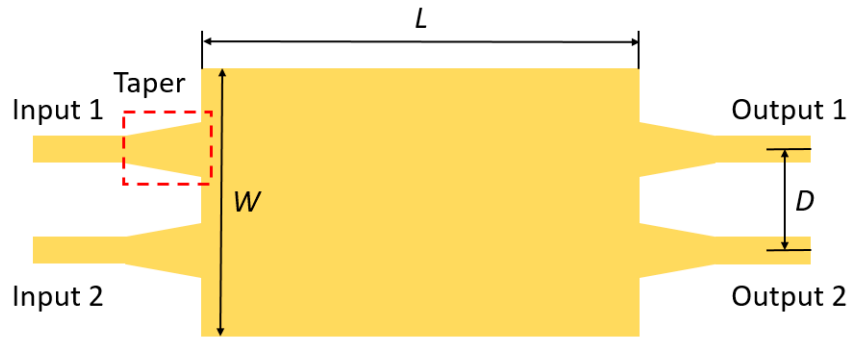
Figure 3. The structure of the MMI coupler.

For a 3 dB 2 × 2 MMI coupler, the length of the multimode waveguide can be calculated as:

$$L = p\frac{L_\pi}{2} \quad p = 1,\ 2,\ 3,\ldots \tag{1}$$

where L_π is the beat length of the two lowest-order modes and can be expressed as:

$$L_\pi = \frac{\pi}{\beta_0 - \beta_1} \approx \frac{4nW_e^2}{3\lambda_0} \tag{2}$$

where β_0 and β_1 are the propagation constants of the fundamental and the first-order lateral modes, respectively, λ_0 is the free-space wavelength, n is the effective refractive index, and W_e is the effective width of the multimode waveguide, which is approximately equal to W [29]. The separation between the input/output ports is $D = W/3$. The width of the multimode waveguide was designed as 9 μm, and the length could be calculated as 98 μm through Equation (1). In order to calculate the exact value of the multimode waveguide length, the optimization was carried out through the beam propagation method (BPM). The relationship between the powers at the two output ports and the multimode waveguide length are illustrated in Figure 4.
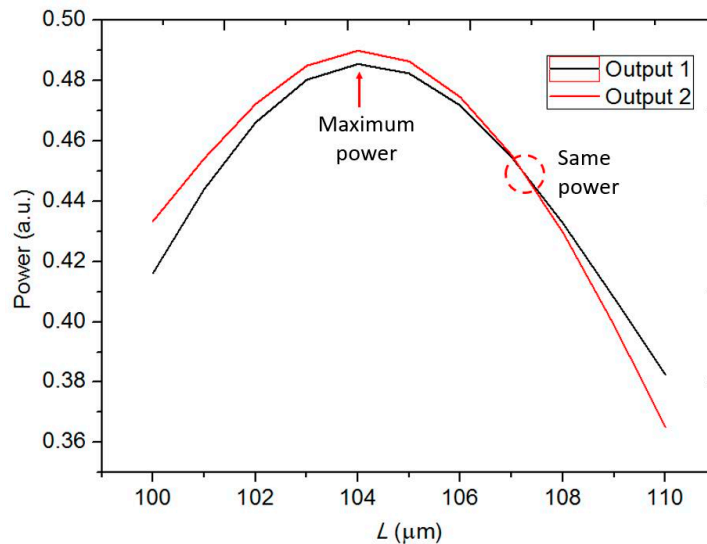

Figure 4. The dependence of two output powers on the length of the multimode waveguide.

It can be seen that both of the output powers increased and then decreased with increasing multimode waveguide length, and that a maximum value existed. The two output powers had the same value at $L = 107$ μm, which is not at the point of maximum values. However, low loss is more important than equal splitting ratio in our work. Therefore, $L = 104$ μm with the maximum values was

chosen as the length of the multimode waveguide. There was a small difference between the result from calculation and simulation. This is because the effective width of the multimode waveguide has been approximated by the multimode waveguide width. As there was an abrupt size change between the single-mode waveguide and the multimode waveguide, there were also scattering loss and reflection loss. Therefore, taper waveguides were designed and optimized to reduce the loss. After simulation, the optimal length and the end width of the taper waveguide were obtained as 10 μm and 1.8 μm. The propagation of the optical field in the MMI coupler is shown in Figure 5.
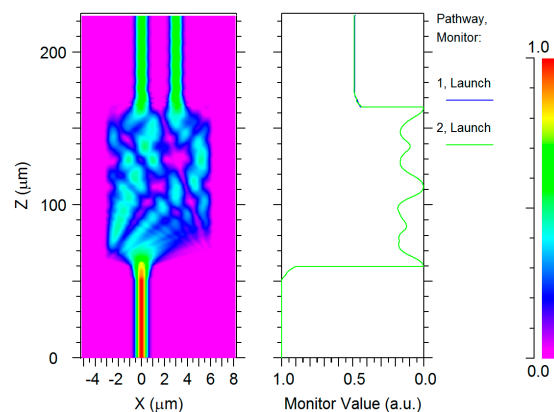

Figure 5. The propagation of the optical field in the MMI coupler with the designed parameters.

3. Fabrication and Characterization

UV Soft NIL, which is considered as cost-effective and allowing high throughput, was applied to fabricate the microring resonator. For conventional NIL, silicon and metal are normally utilized to fabricate the hard mold by etching. However, the etching process will result in surface roughness problems which increase the scattering loss of the waveguide. The hard mold in this article was prepared on a negative photoresist SU8 (MicroChemicals) by UV lithography in order to avoid the etching process. The preparation process can be described as below. First, the silicon wafer which was used as the substrate was carefully cleaned using pirahna and acetone. Before preparing the SU8 film, the Ti-prime (MicroChemicals) was spin-coated on the substrate in order to improve the adhesion and the uniformization of SU8 film. Then, the SU8 was spin-coated on the substrate with the spin speed 5600 rpm (rounds per minutes) for 40 s. The thickness was controlled to be about 980 nm by adjusting the spin-coating parameters. After two steps post-baking (65 °C for 2 min, 95 °C for 2 min), the UV exposure was carried out using the contact mask aligner, Süss MA6, and the high-resolution mask. Then the sample was baked again using the same parameters as mentioned above. After 40 s developing, the patterns could be prepared on the substrate. At last, the thermal curing at 180 °C for 10 min was applied to make SU8 cross-linked and solidified completely.

The fabrication process of the soft mold is illustrated in Figure 6a–c. Before fabrication, the PFPE acrylate should be prepared by mixing Irgacure 2022 photoinitiator (BASF) with Fluorolink MD 700 (Solvay Solexis) at the proportion 1:20. As the viscosity of the PFPE acrylate was not very high, the bubbles could be rejected out by about 20 min standing. Then the PFPE acrylate was cast on the top of the SU8 hard mask. A Polystyrene foil must be placed on the top of the PFPE acrylate in order to improve the mechanical stability. Afterwards, a roller was applied to press the foil in order to make sure the hard mask was fully filled by the PFPE acrylate and the patterns could be perfectly replicated. Different from the thermal curing of a PDMS soft mold, UV curing with 30 mW/cm^2 for 90 s was used for the PFPE soft mold, which simplified the curing process. After peeling off, the PFPE soft mold was prepared.

The imprinting processes are illustrated in Figure 6d–f. The silicon wafer with SiO$_2$ layer on the top was used as the substrate. The SiO$_2$ layer with the thickness of 3 μm acted as the under cladding, which was thick enough to prevent the light leaking out from the waveguide. After carefully

cleaning, the Ormoprime was spin-coated on the substrate in order to improve the adhesion and the uniformization of the OrmoCore layer. The OrmoCore needed to be diluted by the thinner maT with the proportion 1:2.3 in order to reach the desired thickness. Then the mixture was spin-coated on the substrate with 3000 rpm for 30 s, followed by thermal curing at 120 °C for 10 min. Afterwards, the PFPE soft mold was carefully placed on the OrmoCore layer. Extra pressure was not necessary as the capillary force was enough for the imprinting. UV curing was applied with a power of 30 mW/cm^2 for 2 min. After peeling off the soft mold, the patterns could be replicated on the OrmoCore layer. Then, the 150 °C thermal curing was applied for 3 h and the microring resonator was finally fabricated.
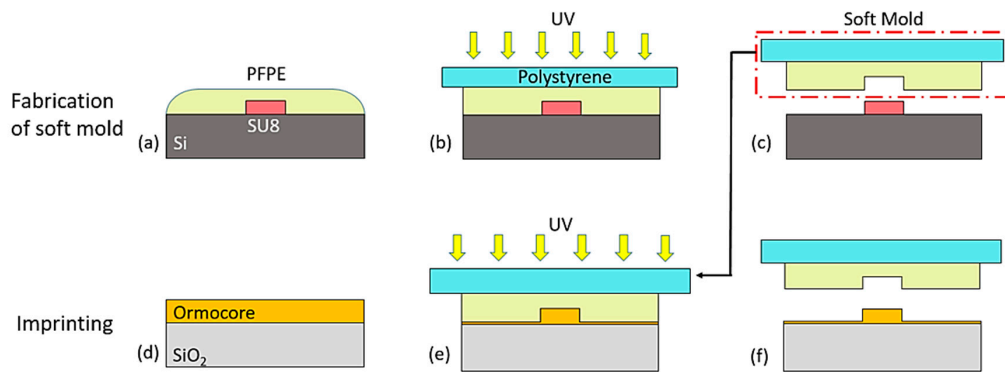

Figure 6. (**a**–**c**) are the fabrication processes of the PFPE soft mold; (**d**–**f**) are the imprinting processes.

The fabricated microring resonator was characterized using scanning electron microscopy. The top views of the entire microring and MMI coupler are shown in Figure 7a,b, respectively. It can be seen that the microring resonator was prepared with UV Soft NIL with good quality. The cross-sections of single-mode waveguide and multimode waveguide are shown in Figure 7b,c. The parameters were almost the same as designed. Figure 7c also shows that the waveguide could be fabricated almost without residual layer. The thickness of the residual layer reached values as low as 40 nm by using "minimum polymer squeezing method" and exploring different monomers (MD 40 and MD 700) [30]. In this article, the proportion between OrmoCore and thinner maT which influences the viscosity is further optimized. After repeated experiments, the optimal proportion 1:2.3 was finally obtained.
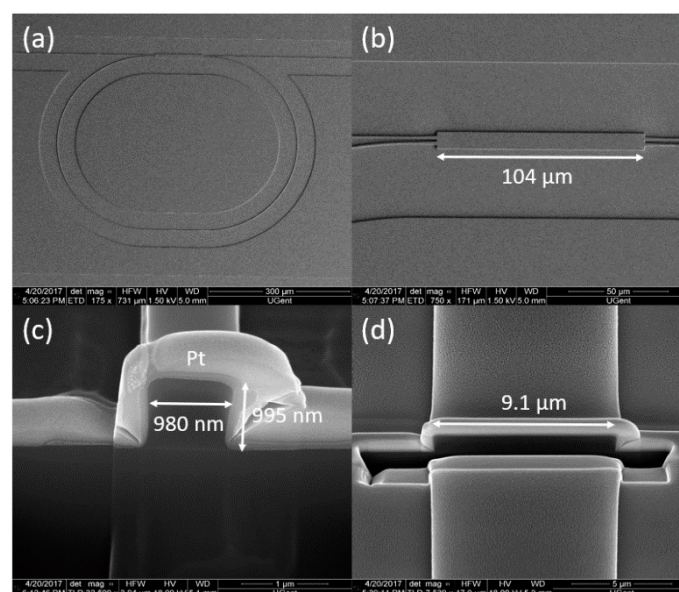

Figure 7. (**a**) Top view of the whole microring resonator; (**b**) Top view of the MMI coupler; (**c**) The cross-section of the single-mode waveguide; (**d**) The cross-section of the multimode waveguide.

4. Measurement and Result Analysis

The schematic of the measurement setup for characterizing the fabricated microring resonator is given in Figure 8. A tunable laser (Newport, with a wavelength range: 890–910 nm and 20 pm resolution) and a power meter were utilized to scan the spectrum of the microring resonator. Since the waveguide was much smaller than the standard fiber, there was a large mode mismatch loss between the polymer waveguide and fiber. In order to solve this problem, the light was launched and collected by tapered lensed fibers. The polarization controllers were applied so as to ensure the whole system operated in the TE mode.
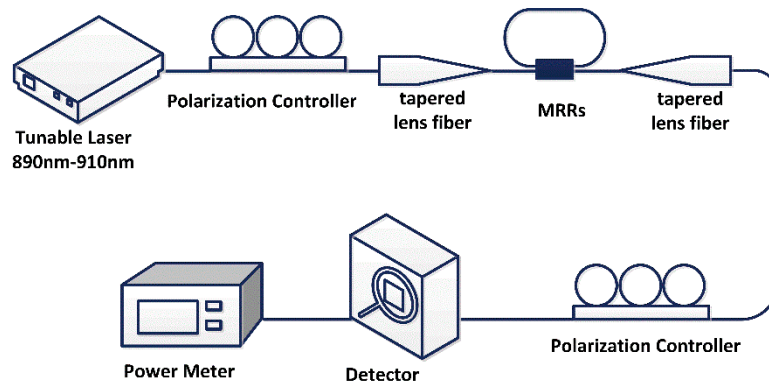

Figure 8. The schematic of the measurement setup.

The measured spectrum of the fabricated microring resonator is shown in Figure 9a. The free spectral range (FSR) and the ER could be obtained as 335 pm and 11.6 dB, respectively. The single peak was fitted by a Lorentz curve and the FWHM (full width at half maximum) was obtained as 39 pm. The Q factor can be calculated through the equation,

$$Q = \frac{\lambda_m}{\text{FWHM}} \tag{3}$$

where λ_m is the resonance wavelength. Then the Q factor could be obtained as 2.3×10^4.
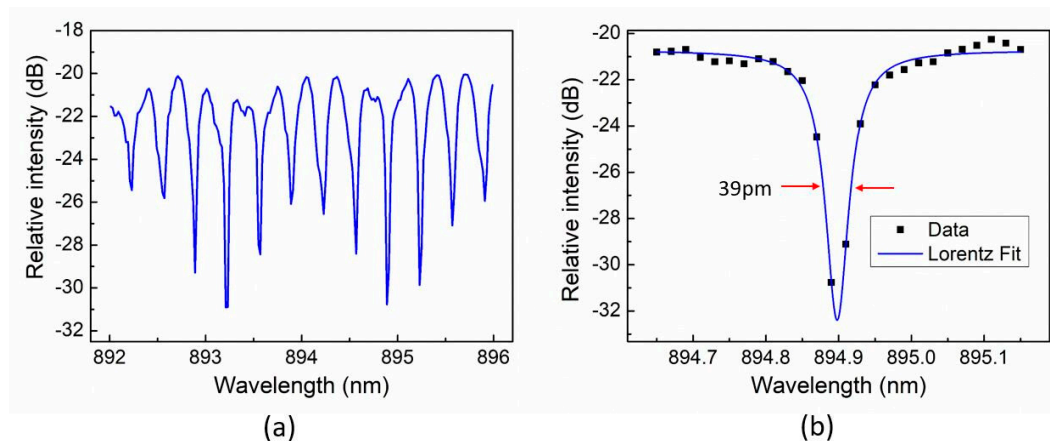

Figure 9. (**a**) Optical transmission spectrum of the fabricated microring resonator under TE mode; (**b**) Lorentzian fit of the single resonance peak.

5. Conclusions

A microring resonator was demonstrated on the cost-effective polymer platform. An MMI structure which has good fabrication tolerance was designed to couple the light between the microring and the straight waveguide. The polymer material, OrmoCore, which has a low absorption loss at

short wavelengths was utilized. The radius and the structure of the MMI coupler were simulated and optimized using 3D BPM in order to reduce the total loss of the microring resonator. The microring resonator was prepared using a UV Soft NIL which is considered as low cost, with high throughput and high resolution. A new material, PFPE, which has very low surface energy was utilized to fabricate the soft mold instead of the PDMS material. The thickness of the residual layer was further reduced by optimizing the proportion of OrmoCore and its thinner maT. The fabricated microring resonator worked at about 890 nm, where the water absorption loss was low, and the lasers and the detectors were also cheap. The transmission was measured by a tunable laser and a power meter. The spectrum with 335 pm FSR and 11.6 dB ER was obtained. The Q factor as high as 2.3×10^4 has been shown.

Author Contributions: Conceptualization, H.L.; methodology, Y.L.; software, H.L.; validation, Z.W., and X.H.; formal analysis, H.L. and Y.L.; investigation, M.Z.; resources, G.M. and M.Z.; data curation, H.L.; writing—original draft preparation, H.L.; writing—review and editing, Y.L. and G.M.; visualization, H.L.; supervision, Y.L.; project administration, Z.W.; funding acquisition, M.Z.

Conflicts of Interest: All authors declare that they have no conflict of interest.

References

1. Jayatilleka, H.; Murray, K.; Caverley, M.; Jaeger, N.A.F.; Chrostowski, L.; Shekhar, S. Crosstalk in SOI Microring Resonator-Based Filters. *J. Lightwave Technol.* **2016**, *34*, 2886–2896. [CrossRef]

2. Qiu, H.; Zhou, F.; Qie, J.; Yao, Y.; Hu, X.; Zhang, Y.; Xiao, X.; Yu, Y.; Dong, J.; Zhang, X. A Continuously Tunable Sub-Gigahertz Microwave Photonic Bandpass Filter Based on an Ultra-High-Q Silicon Microring Resonator. *J. Lightwave Technol.* **2018**, *36*, 4312–4318. [CrossRef]

3. Dubé-Demers, R.; St-Yves, J.; Bois, A.; Zhong, Q.; Caverley, M.; Wang, Y.; Chrostowski, L.; LaRochelle, S.; Plant, D.V.; Shi, W. Analytical Modeling of Silicon Microring and Microdisk Modulators with Electrical and Optical Dynamics. *J. Lightwave Technol.* **2015**, *33*, 4240–4252. [CrossRef]

4. Chang, C.-M.; de Valicourt, G.; Chandrasekhar, S.; Dong, P. Differential Microring Modulators for Intensity and Phase Modulation: Theory and Experiments. *J. Lightwave Technol.* **2017**, *35*, 3116–3124. [CrossRef]

5. Arbabi, A.; Kamali, S.M.; Arbabi, E.; Griffin, B.G.; Goddard, L.L. Grating integrated single mode microring laser. *Opt. Express* **2015**, *23*, 5335–5347. [CrossRef] [PubMed]

6. Sui, S.-S.; Tang, M.-Y.; Yang, Y.-D.; Xiao, J.-L.; Du, Y.; Huang, Y.-Z. Investigation of hybrid microring lasers adhesively bonded on silicon wafer. *Photonics Res.* **2015**, *3*, 289–295. [CrossRef]

7. Vos, K.D.; Bartolozzi, I.; Schacht, E.; Bienstman, P.; Baets, R. Silicon-on-Insulator microring resonator for sensitive and label-free biosensing. *Opt. Express* **2007**, *15*, 7610–7615. [CrossRef]

8. Mi, G.; Horvath, C.; Aktary, M.; Van, V. Silicon microring refractometric sensor for atmospheric CO(2) gas monitoring. *Opt. Express* **2016**, *24*, 1773–1780. [CrossRef]

9. Wang, L.; Ren, J.; Han, X.; Claes, T.; Jian, X.; Bienstman, P.; Baets, R.; Zhao, M.; Morthier, G. A label-free optical biosensor built on a low-cost polymer platform. *IEEE Photonics J.* **2012**, *4*, 920–930. [CrossRef]

10. Shahoei, H.; Xu, D.X.; Schmid, J.H.; Yao, J. Photonic fractional-order differentiator using an soi microring resonator with an MMI coupler. *IEEE Photonics Technol. Lett.* **2013**, *25*, 1408–1411. [CrossRef]

11. Xu, D.X.; Vachon, M.; Densmore, A.; Ma, R.; Schmid, J.H. Label-free biosensor array based on silicon-on-insulator ring resonators addressed using a WDM approach. *Opt. Lett.* **2010**, *35*, 2771–2773. [CrossRef] [PubMed]

12. Ymeti, A.; Kanger, J.S.; Greve, J.; Lambeck, P.V.; Wijn, R.; Heideman, R.G. Realization of a multichannel integrated Young interferometer chemical sensor. *Appl. Opt.* **2003**, *42*, 5649–5660. [CrossRef] [PubMed]

13. Ksendzov, A.; Lin, Y. Integrated optics ring-resonator sensors for protein detection. *Opt. Lett.* **2005**, *30*, 3344–3346. [CrossRef] [PubMed]

14. Maxwell, A.; Huang, S.W.; Ling, T.; Kim, J.S.; Ashkenazi, S.; Guo, L.J. Polymer microring resonators for high-frequency ultrasound detection and imaging. *IEEE J. Sel. Top. Quantum Electron.* **2008**, *14*, 191–197. [CrossRef] [PubMed]

15. Salleh, M.H.M.; Glidle, A.; Sorel, M.; Reboud, J.; Cooper, J.M. Polymer dual ring resonators for label-free optical biosensing using microfluidics. *Chem. Commun.* **2013**, *49*, 3095. [CrossRef] [PubMed]

16. Girault, P.; Lorrain, N.; Poffo, L.; Guendouz, M.; Lemaitre, J.; Carré, C.; Gadonna, M.; Bosc, D.; Vignaud, G. Integrated polymer micro-ring resonators for optical sensing applications. *J. Appl. Phys.* **2015**, *117*, 104504. [CrossRef]

17. Rezem, M.; Günther, A.; Roth, B.; Reithmeier, E.; Rahlves, M. Low-Cost Fabrication of All-Polymer Components for Integrated Photonics. *J. Lightwave Technol.* **2017**, *35*, 299–308. [CrossRef]

18. Shi, F.; Bamiedakis, N.; Vasil'ev, P.P.; Penty, R.V.; White, I.H.; Chu, D. Flexible multimode polymer waveguide arrays for versatile high-speed short-reach communication links. *J. Lightwave Technol.* **2018**, *36*, 2685–2693. [CrossRef]

19. Ma, H.; Jen, A.K.Y.; Dalton, L.R. Polymer-based optical waveguides: Materials, processing, and devices. *Adv. Mater.* **2010**, *14*, 1339–1365. [CrossRef]

20. Eldada, L.; Shacklette, L.W. Advances in polymer integrated optics. *IEEE J. Sel. Top. Quantum Electron.* **2000**, *6*, 54–68. [CrossRef]

21. Kirchner, R.; Finn, A.; Landgraf, R.; Nueske, L.; Teng, L.; Vogler, M.; Fischer, W.-J. Direct UV-Imprinting of Hybrid-Polymer Photonic Microring Resonators and Their Characterization. *J. Lightwave Technol.* **2014**, *32*, 1674–1681. [CrossRef]

22. Zgraggen, E.; Soganci, I.M.; Horst, F.; Porta, A.L.; Dangel, R.; Offrein, B.J.; Snow, S.A.; Young, J.K.; Swatowski, B.W.; Amb, C.M.; et al. Laser direct writing of single-mode polysiloxane optical waveguides and devices. *J. Lightwave Technol.* **2014**, *32*, 3036–3042. [CrossRef]

23. Ting, H.; Steve, M.; Mathew, Z.; Robbie, C.; Barry, L.D. Low loss high index contrast nanoimprinted polysiloxane waveguides. *Opt. Express* **2009**, *17*, 2623.

24. Goh, S.J.; Bastiaens, H.J.M.; Vratzov, B.; Huang, Q.; Bijkerk, F.; Boller, K.J. Fabrication and characterization of free-standing, high-line-density transmission gratings for the vacuum UV to soft X-ray range. *Opt. Express* **2015**, *23*, 4421–4434. [CrossRef] [PubMed]

25. Han, X.Y.; Wu, Z.L.; Yang, S.C.; Shen, F.F.; Liang, Y.X.; Wang, L.H.; Wang, J.Y.; Ren, J.; Jia, L.Y.; Zhang, H. Recent Progress of Imprinted Polymer Photonic Waveguide Devices and Applications. *Polymers* **2018**, *10*, 603. [CrossRef] [PubMed]

26. Williams, S.S.; Retterer, S.; Lopez, R.; Ruiz, R.; Samulski, E.T.; Desimone, J.M. High-Resolution PFPE-based Molding Techniques for Nanofabrication of High-Pattern Density, Sub-20 nm Features: A Fundamental Materials Approach. *Nano Lett.* **2010**, *10*, 1421–1428. [CrossRef] [PubMed]

27. Jacob, J.; Yuying, T.; Rothstein, J.P.; Watkins, J.J.; Carter, K.R. Large-area, continuous roll-to-roll nanoimprinting with PFPE composite molds. *Nanotechnology* **2013**, *24*, 505307.

28. Hiltunen, M.; Hiltunen, J.; Stenberg, P.; Petäjä, J.; Heinonen, E.; Vahimaa, P.; Karioja, P. Polymeric slot waveguide at visible wavelength. *Opt. Lett.* **2012**, *37*, 4449–4451. [CrossRef]

29. Soldano, L.B.; Pennings, E.C.M. Optical Multi-Mode Interference Devices Based on Self-Imaging: Principles and Applications. *J. Lightwave Technol.* **1995**, *13*, 615–627. [CrossRef]

30. Morarescu, R.; Pal, P.; Beneitez, N.; Missinne, J.; Steenberge, G.; Bienstman, P.; Morthier, G. Fabrication and characterization of high-optical-quality-factor hybrid polymer microring resonators operating at very near infrared wavelengths. *IEEE Photonics J.* **2016**, *8*, 1–9. [CrossRef]